Journal of Physics D: Applied Physics

PAPER • **OPEN ACCESS**

Defect characterization of heavy-ion irradiated AlInN/GaN on Si high-electron-mobility transistors

To cite this article: S R Challa *et al* 2022 *J. Phys. D: Appl. Phys.* **55** 115107

View the article online for updates and enhancements.

You may also like

- ^{60}Co -rays irradiation effect in DC performance of AlGaN/GaN high electron mobility transistors
Gu Wenping, Chen Chi, Duan Huantao et al.

- Applications of AlGaN/GaN high electron mobility transistor-based sensors in water quality monitoring
Hui Guo, Xiuling Jia, Yan Dong et al.

- Performance of an AlGaN/GaN MISHEMT with sodium beta-alumina for gate insulation and surface passivation
Benlang Tian, , Chao Chen et al.

ECS Membership = Connection

ECS membership connects you to the electrochemical community:

- Facilitate your research and discovery through ECS meetings which convene scientists from around the world;
- Access professional support through your lifetime career:
- Open up mentorship opportunities across the stages of your career;
- Build relationships that nurture partnership, teamwork—and success!

Join ECS! Visit electrochem.org/join

This content was downloaded from IP address 141.44.170.14 on 05/08/2022 at 09:17

OPEN ACCESS
IOP Publishing

Journal of Physics D: Applied Physics

J. Phys. D: Appl. Phys. **55** (2022) 115107 (7pp)

https://doi.org/10.1088/1361-6463/ac40b8

Defect characterization of heavy-ion irradiated AlInN/GaN on Si high-electron-mobility transistors

S R Challa[1], H Witte[1,*], G Schmidt[1], J Bläsing[1], N Vega[3], C Kristukat[4], N A Müller[2], M E Debray[2], J Christen[1], A Dadgar[1] and A Strittmatter[1]

[1] Institut für Physik, Otto-von-Guericke-Universität Magdeburg, Magdeburg, Germany
[2] Gerencia de Investigación y aplicaciones, Comisión Nacional de Energía Atómica, San Martin 1650, Argentina
[3] Laboratorio Argentino de Haces de Neutrones Comisión Nacional de Energía Atómica, San Martin 1650, Argentina
[4] ECyT, Universidad de San Martín, 1650 San Martín, Argentina

E-mail: hartmut.witte@ovgu.de

Received 3 September 2021, revised 4 November 2021
Accepted for publication 7 December 2021
Published 20 December 2021

Abstract

The characteristic energies of traps in InAlN/AlN/GaN high-electron mobility transistor structures on Si(111) substrates formed after irradiation with 75 MeV S-ions are studied by means of c-lattice parameter analysis, vertical IV-characteristics, micro-photoluminescence (μ-PL), photocurrent (PC) and thermally stimulated current (TSC) spectroscopy. From the lattice parameter analysis, point defect formation is concluded to be the dominant source of defects upon irradiation. A strong compensation effect manifests itself through enhanced resistivity of the devices as found in vertical IV-measurements. Defect formation is detected optically by an additional PL-band within the green spectral region, while defect states with threshold energies at 2.9 eV and 2.65 eV were observed by PC spectroscopy. The TSC spectra exhibit two defect-related emissions between 300 K and 400 K with thermal activation energies of 0.78–0.82 eV and 0.91–0.98 eV, respectively. The data further supports the formation of Ga vacancies (V_{Ga}) and related complexes acting mainly as acceptors compensating the originally undoped n-type GaN buffer layers after irradiation.

Keywords: gallium nitride, high electron mobility transistor, deep defects, ion irradiation, optical and electrical defect spectroscopy

(Some figures may appear in colour only in the online journal)

1. Introduction

InAlN/GaN high electron mobility transistors (HEMT) structures are attractive for power operation as lattice-matched InAlN/GaN interfaces exhibit very large sheet electron densities and, consequently, low channel resistivity [1]. These HEMTs also include an ultra-thin AlN spacer layer for further improvement of the conductivity of the channel region. High quality epitaxial growth of these structures can be realized on large size Si(111) substrates by metalorganic vapor-phase epitaxy (MOVPE), which is attractive as an economically prospective technology for GaN-based HEMT transistors [2]. Studies have shown that for GaN on Si HEMTs vertical leakage current associated defects in the buffer layer limit breakdown voltage [3].

* Author to whom any correspondence should be addressed.

Original content from this work may be used under the terms of the Creative Commons Attribution 4.0 licence. Any further distribution of this work must maintain attribution to the author(s) and the title of the work, journal citation and DOI.

Distinct epitaxial designs of GaN-based lateral HEMT device structures can be realized by different epitaxial growth techniques and a final choice with regard to, for instance, space applications demand a detailed analysis of radiation-induced changes of their characteristics.

Radiation hardness of high power and/or high frequency electron transistors is a primary requirement for space applications [4]. GaN based HEMTs have previously shown great potential for power and high frequency operation, simultaneously exhibiting superior radiation hardness as compared to Si and GaAs-based devices [5].

The larger interatomic binding in GaN leads to higher thresholds for damage during irradiation. Nevertheless, defect formation will take place for particle energies exceeding these thresholds. Radiation induced point defect formation can therefore be expected also for GaN-based HEMTs operating in space or other applications with high radiation fields [6]. Charged point defects will have an impact on HEMT characteristics such as breakdown voltage, threshold voltage and saturation current depending on the layer structure and the device layout [7].

Multiple charged, heavy ions are known to produce structural nano-holes and nano-hillocks within GaN layers and/or at the surface, respectively [8]. Surface etching due to 308 MeV Xe ions as well as homogeneous lattice expansion has also been reported [9]. By using Au, the formation of dislocations, defect clusters, and traps may occur in the epitaxial layers [10]. In the case of singly charged ion irradiation, intrinsic point defects were seen to reduce the free carrier concentration by compensation effects [11] up to a complete isolation of GaN layers [12]. Interface defects were also found in GaN based HEMTs or diodes [13].

Under the conditions of 75 MeV sulfur ion irradiation into GaN layers, the dominant energy loss process is the electronic loss in contrast to the nuclear stopping process described in [7] and [8]. As a consequence, the damage processes in GaN involve more excitations of the electron clouds than of atom displacements [7].

As we reported recently, compensation effects upon irradiation lead to highly resistive buffer layers [14]. The impact of the compensated buffer layer on the transfer characteristics of the HEMTs has been already discussed in [14].

In the present paper, we study the defect formation mechanism by analyzing the lattice constants of the GaN buffer layer by x-ray diffraction (XRD) and trap related energies using micro-photoluminescence (μ-PL) spectroscopy in the device region of irradiated HEMT structures as well as photo-current (PC) and thermally stimulated current (TSC) spectroscopy of these structures. By comparing the observed characteristics with those of previously reported defects, the formation of Ga vacancies and related complexes is confirmed.

2. Experiment

The samples were grown by MOVPE in an AIXTRON AIX200/4 RF-S MOVPE reactor using standard precursors. Highly conductive n^{++}-Si(111) was chosen as the substrate. The layer structure comprises an AlN/AlGaN/GaN sequence wherein the threading dislocation density was reduced and the stress of the layer stack was adjusted to avoid cracks upon cooling to room temperature. The actual device layer structure follows an undoped, 1.5 μm thick GaN buffer on which the barrier layer sequence consisting of 1.5 nm AlN and 10 nm Al $_{0.87}$ In $_{0.13}$ N was grown. Finally, a thin GaN cap and a SiN_x insulation layer were applied as is shown in figure 1.

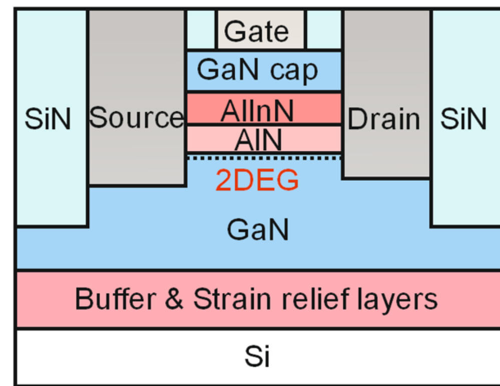

Figure 1. Schematic cross section of the investigated AlInN/AlN/GaN HEMTs heterostructures (for more details see [8]).

Dual-finger gate and depletion mode HEMTs were structured with Ohmic contacts using an alloyed Ti/Al/Ni/Au (20/50/14/60 nm) metal stack on the surface and a Ni/Au gate contact. All five dual-gate HEMTs used here were isolated against each other by the SiN_x passivation layer. The HEMT structure as well as the contact formation are described in detail in [14].

Dual-finger gate and depletion mode HEMTs were structured with gate width and length of $W_G = 50$ μm and $L_G = 1.5$ μm, respectively, and with source-gate and source-drain spacing of $S_G = 1.5$ μm and $S_D = 4.5$ μm, respectively. Each HEMT has a dimension of 650×450 μm^2.

The 75 MeV sulfur ion irradiation experiments were performed at room temperature in the heavy ion Microbeam (MiP) line of the TANDAR accelerator in Buenos Aires, Argentina. The MiP features a focusing and scanning system for high-energy heavy S-ions at normal incidence allowing for a spatial resolution of about 500×500 μm^2 centered around the gate area of each dual gate HEMT. The whole irradiation equipment is explained in more detail in [12, 14].

A chip area was selected for the irradiation experiments where five dual-finger gate HEMTs arranged in a row and separated by 50 μm from each other. These five devices were irradiated with 75 MeV sulfur ions at fluences of 7.05×10^{13}, 3.4×10^{14}, none, 6.97×10^{14}, and 1.4×10^{15} ions cm^{-2}, respectively.

Devices were chip-mounted, including wire-bonding of the gate contacts using a 25 μm diameter Al wire and an electrical contact to the backside of the Si substrate. These chip-mounted devices were placed in a cryostat for electrical measurements between the gate contacts and the substrate.

The conductive Si-substrate served as the backside contact for all used HEMTs and was connected from the bottom of the chip carrier by silver conducting paste.

All the investigated HEMTs showed identical I_{DS}–V_{DS}- and I_{DS}–V_{GS}-characteristics before irradiation measured at room temperature using an SCS 4200 characterization system from Keithley Instruments. The contact resistance between the needle probe and the gate contact was negligible compared to the sample resistance.

Taking into account layer thickness, both the Si-substrate and the GaN buffer layers contribute to the electrical responses. Since both the silicon substrate and the GaN buffer have strongly differing optical absorption and emission spectra and different thermally activated electrical behavior, their signature within photocurrent, photoluminescence or thermal stimulated current spectroscopy can be easily separated.

High-resolution x-ray diffraction (HR-XRD) measurements in Θ/2Θ-scan mode were used to investigate any change in the *c*-lattice parameter after irradiation. We also used a GaN (0002) ω-scan to observe changes in the coherence length and tilt of the crystalline layers. Each irradiated HEMT could be assessed individually using a spatially resolving HR-XRD setup (Rigaku SmartLab μHR). The lattice strain in the *c*-direction is measured as $(c_{meas} - c_{rel})/c_{rel}$, taking the relaxed lattice constant in the *c*-direction (*c*-value) as 5.1855 Å after [13].

μ-PL measurements were performed at 4 K with a He-Cd laser operating at 325 nm wavelength. The spot diameter was nearly one micrometer and located between the source and drain contacts of each HEMT structure. A calibrated white light source allowed us to de-convolute the spectral transfer characteristics of the optical setup.

PC spectroscopy of the samples under vacuum conditions was realized by front side illumination in the wavelength range between 250 nm and 600 nm using a 30 W Xe-lamp and a Spectra Pro 300 monochromator from Acton Research at room temperature. The total incident photon dose was measured by placing a calibrated UV-enhanced bolometer at the sample position. For these wavelength regions, the bolometer signals are kept spectrally independent by using a quartz window.

TSCs can be measured when traps are filled with charge carriers at low temperatures that are re-emitted from the traps upon heating in dark ambient. We used high-intensity UV light from a mercury lamp to generate charge carriers at 80 K for the initial trap filling process and heated the samples under vacuum in a cryostat setup up to temperatures of 400 K. Each TSC spectrum is obtained by subtracting a non-stimulated (or dark) spectrum from the optically stimulated spectrum. If persistent photocurrents were strong, the samples are shown only up to 200 K. For the non-irradiated and irradiated samples, the bias was set at 5 V and 10 V, respectively, yielding comparable current densities in both samples.

3. Results and discussion

In our previous work, atomic displacement effects upon sulfur irradiation were already simulated using a so-called stopping and range of ions in matter (SRIM) software tool (see [14, 15]). The estimated ion stopping range is 21 μm.

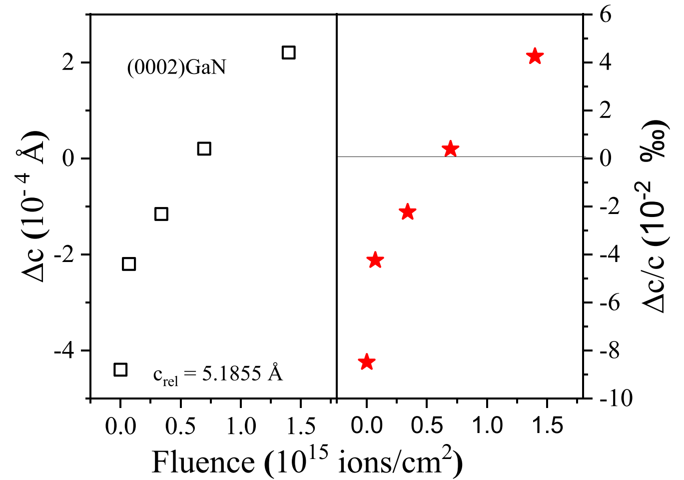

Figure 2. Expansion of the GaN *c*-lattice constant as determined from GaN Θ/2Θ-HRXRD measurements (left) and the corresponding *c*-lattice strain (right) in dependence of the irradiation fluence.

The measured *c*-lattice parameters shown in figure 2 depend strongly on the fluence of the S-ion irradiation. While the non-irradiated HEMT showed a nearly relaxed value for the *c*-lattice constant (a moderate tensile thermal strain is typical for our GaN- on -Si(111) structures), an increased value was obtained with increasing fluence. This can be explained by irradiation-induced point defects due to stopping processes at this ion energy /7/ leading to a slight expansion in the c-direction of the GaN lattice. Similar results were also reported in [16] using 180 keV Ar and Ca ions. There, the lattice mismatch was between (0.001–0.009) ‰ and (0.003–0.014) ‰ for Ca-ions and Ar-ions, respectively, according to fluences between 10^{13} to 2×10^{15} ions cm^{-2}. Such lattice expansion detected by HR-XRD also occurred in [9, 17] where irradiation with 308 MeV Xe-ions or implantation processes with different ions and fluences were studied, respectively. For higher ion energies, both surface damage recognized by atomic force microscopy and changes in the a-lattice constant in HR-XRD are to be expected. The latter kind of damage implies biaxial and hydrostatic strain, leading to tilt and dislocation generation as reported in [9]. For multiple charged ions with high fluence, strong structural damage by nuclear energy losses should be small for the used sulfur ion energy as seen in [7] and [8].

In contrast, (0002) ω-scans in HR-XRD taken on S-irradiated structures yield full width at half maximum (FWHM)-values of (315 ± 1.8) arcsec independent of the fluence. Therefore, coherence length in the *a*-direction as well as any tilt and dislocation density has not changed upon heavy ion irradiation and formation of extended defects such as dislocations or grain boundaries can be excluded.

Additionally, atomic force microscopy measurements of the SiN_x surfaces of all HEMTs showed no discernable changes in the surface roughness (about 1.0 ± 0.3) nm with increasing fluence, which suggests unchanged surface properties and negligible damage to the layer surfaces.

The vertical IV-characteristics between substrate and gate electrode are shown in figure 3. For HEMTs irradiated with the

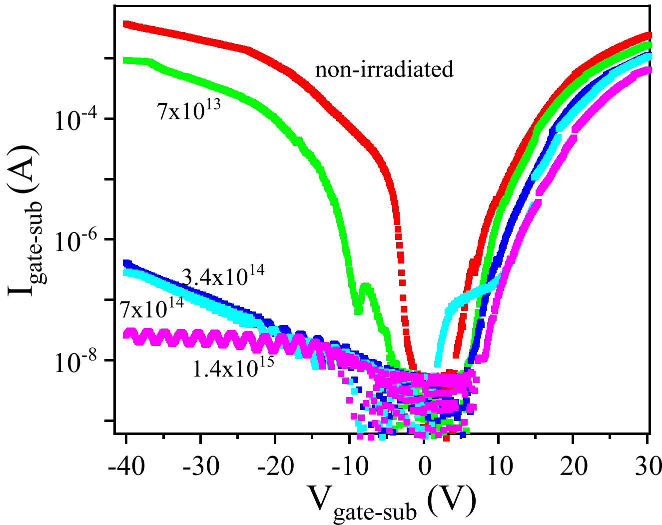

Figure 3. IV- characteristics of current transport between Si-substrate and gate contact for all irradiated HEMTs revealing a reduction of reverse and of forward currents.

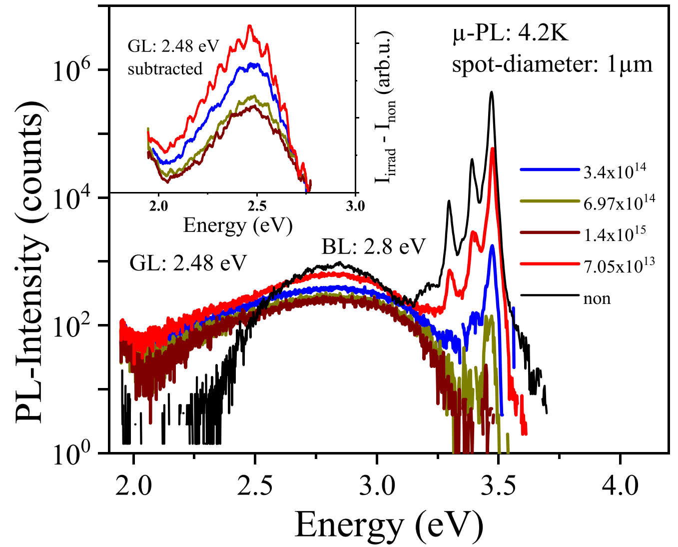

Figure 4. μ-PL spectra of all samples at 4.2 K. Donor-bound exciton (DBE) emission with its longitudinal optical phonon replica ($-$1LO/$-$2LO) is strongly reduced whereas blue band luminescence (BL) decreases weakly in intensity with higher fluence. The inset shows irradiation induced green band luminescence (GL).

highest dose, the characteristics are typical for Schottky-type heterojunctions with forward and depletion current regions. In contrast, the non-irradiated sample and the one with the lowest dose exhibited weak rectifying behavior in forward as well as in reverse (depletion) directions. This behavior of the non or weakly irradiated HEMT was due to high intrinsic reverse currents caused by the high free carrier concentration of the GaN buffer resulting in a small depletion region of the rectifying gate/InAlN/undoped GaN buffer contact. With increasing fluence, the series resistance obtained from the forward region increases by about one order of magnitude and the resistivity of the depletion region rises by about five orders of magnitude.

We determined the non-irradiated, undoped buffer GaN layer to be n-type conductive with residual donor concentrations in the low 10^{16} cm^{-3} range from capacitance-voltage-measurements between gate and back contacts. Since all HEMTs investigated here shown to have nearly identical vertical IV-characteristics before irradiation, the increase in resistivity of the 10^{14} ion cm^{-2} irradiated HEMT corresponds to changes in the transfer characteristics of the devices without and with irradiation, as reported in [14].

The ion stopping range is 21 μm estimated by the SRIM calculations [12]. Therefore, the ions reach the Si-substrate and introduce deep defects. However, the Si-substrates were highly doped with a free carrier concentration of nearly 10^{19} cm^{-3} which is hard to compensate. Additionally, a high resistive Si substrate should leave an optical absorption edge within the photocurrent spectra below 1.1 eV, which was not observed. Therefore, the rectifying IV-characteristics represent the metal—gate/InAlN/GaN contact with the depletion range within GaN. As a consequence, irradiation induced compensation of free electrons causes enhancement of resistivity by acceptors. This electrical insulation or carrier reduction of n-type GaN layers upon MeV ion irradiation is well known, from [11, 18], for instance. Strong damage within the gate/InAlN/GaN channel part of the HEMTs was not observed in the HEMT transfer characteristics [14].

μPL measurements were performed on all samples displayed in figure 4. The spectrum of the non-irradiated HEMT exhibits a strong and dominant emission within the near band edge (NBE) region of GaN at 3.471 eV, mainly recombination of donor-bound excitons (DBE) [19]. These peaks are accompanied by longitudinal-optical phonon replica at about 3.39 eV and 3.29 eV. The weak shoulder at 3.24 eV may originate from donor-acceptor pair recombination [19]. As can be seen, a broad blue luminescence (BL) band occurs at $\sim$2.85 eV.

For irradiated samples, NBE intensity is strongly reduced with increasing fluence. Compared to the reference sample, DBE peak intensity is almost one order of magnitude less for 7.1 $\times$ 10^{13} ions cm^{-2} and reaches the noise level for the highest irradiated sample. The BL also occurs for irradiated samples, but its peak intensity decreases with higher fluence only weakly compared to NBE, like in [12], and remains constant in spectral position.

Moreover, ion irradiation induces an additional emission at lower energies overlapping with the BL. This additional feature has been magnified by subtracting the PL spectrum of the non-irradiated sample normalized to BL peak intensity (see inset figure 4). Thereby, a green luminescence (GL) band at $\sim$2.5 eV is revealed. With increasing ion fluence, the GL intensity decreases only weakly.

In GaN layers, the GL usually occurs in combination with a yellow luminescence band (YL). Both emission bands show different saturation effects with enhanced excitation intensity [19, 20]. The origin of YL and GL was discussed in [20] as a radiative recombination to different charge states of the acceptor-like V_{Ga}–O_N complex. Based on theoretical studies [21], other hole capture processes of acceptors such as N_{Ga}^-,

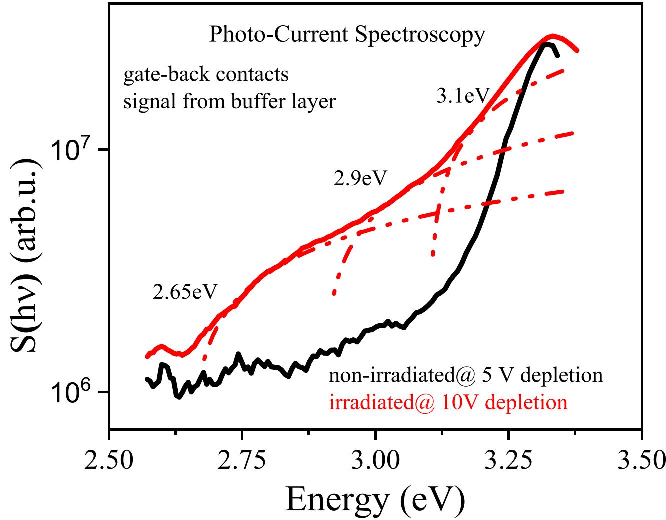

Figure 5. Optical response of photocurrent versus photon energy for the non-irradiated and the irradiated sample with the highest dose at room temperature. Dotted lines represent spectral contributions by deep defect absorption processes (for details see text).

N_i^0 and V_{Ga}^{-3} defects are further candidates for emissions at 2.54 eV, at 2.49 eV, and at 2.35 eV, respectively.

In as-grown GaN epilayers, only YL at 2.2 eV and neither BL or GL were reported [9]. After irradiation with 308 MeV Xe-ions, YL vanished and BL at 2.75 eV as well as GL at 2.4 eV that appeared while their intensities were not affected by higher fluence.

In our as-grown undoped buffer layer, the occurrence of BL and the absence of YL indicates the presence of only shallow acceptor levels, such as Mg, C, or Zn as well as low concentrations of intrinsic deep acceptors [19]. After 75 MeV S-ion irradiation, the concentrations of shallow acceptors remained virtually unchanged since the BL intensity remained constant. However, the appearance of GL is strong evidence for intrinsic defect generation acting as deep acceptors and, therefore, compensated by the *n*-type conductive buffer layer towards highly resistive behavior. Due to the associated Fermi level shift towards the mid-gap, the involved acceptor-like traps can be assumed to be in a new charge state triggering the occurrence of GL instead of the YL band.

Figure 5 shows the optical response of the irradiation series obtained from photo-current spectroscopy below the GaN absorption edge at about 3.4 eV. The absolute optical response is 20 times higher for the non-irradiated HEMT as compared to the irradiated samples, which indicates strong trap incorporation strongly reducing the overall optical response.

The optical response function S of the HEMTs used here is defined as $S = (I_{ph} - I_0)/I_0) \times P(h\nu)$ with I_{ph} being the measured photo-current at fixed bias, I_0 dark current and $P(h\nu)$ the spectral optical power.

Near band gap peaks in the photo-current spectra in figure 5 appear at 3.33 eV, which differs strongly from the room-temperature band gap edge at about 3.45 eV. This is caused by strong non-radiative recombination at the surface. Due to the low penetration depth of light with wavelengths close to the absorption edge, strong non-radiative surface recombination dominates and reduces the PC signal even though absorption is strong (see also [22]). At longer wavelengths with lower but non-zero absorption by GaN light penetration expands into deeper sections and, therefore, a PC peak can be observed below the absorption edge.

Under the condition of a weak generation rate (low excitation power density) the optical response S is related to the photo-ionization cross-section of deep defects σ with $\sigma \approx K\ (h\nu - E_{trap})^{1/2}$ after [22]. Here, K is a constant including the trap density, the photon-energy $h\nu$ and E_{trap} represents the energy difference of the trap state to the respective band into which the carrier is emitted.

The curve of the non-irradiated sample is featureless at energies around 3.1 eV, 2.9 eV and 2.65 eV, whereas the spectral response curves of the irradiated sample clearly exhibit steps at those energies. Accordingly, the spectra of the irradiated samples were fitted with three respective absorption states as indicated by dash-dotted lines in figure 5. The appearance of these defect-related absorption states upon irradiation is another consequence of the defect formation.

Absorption-related thresholds for emission from traps have been found in as-grown GaN-field effect transistor (FET)s at 3.2 eV, 2.85 eV and 1.8 eV by photoionization spectroscopy [23, 24] and also at 3.28 eV, 2.62 eV and 1.28 eV by drain-current deep-level optical spectroscopy [25]. Because of a limited sensitivity below 1.8 eV, the 1.28 eV absorption was not detectable in our measurement. The absence of the 2.8 eV-related absorption might be due to a significantly lower response than for the 2.9 eV and 2.65 eV states. However, reported peak energies at 2.85 eV and 2.62 eV are also present in the PC spectra shown in figure 5. Defect-induced photon absorption at 2.85 eV has been discussed as caused by a deep acceptor-like carbon defect at about $E_V + 0.8$ eV in [23], as related to an AlGaN surface state in [24] or as due to a V_{Ga}–H–O complex in [26]. A 2.64 eV transition, which is similar to our threshold at 2.65 eV, was interpreted as Ga vacancy [25]. All observed photoluminescence and photocurrent peaks in our samples as well as their interpretations with regard to literature are summarized in table 1.

As we can exclude any carbon incorporation upon irradiation, the threshold at 2.9 eV must be assigned to V_{Ga}-related complexes such as V_{Ga}–O–H rather than to a carbon acceptor. This is supported by the energies of the main trap absorption confirming V_{Ga} generation during irradiation.

Figure 6 shows TSC spectra of the non-irradiated HEMT. Thermal defect emissions appear only above 250 K with two peaks at 260–270 K (A) and 300 K (B). Above 320 K only detector noise was observed (magnified by ten).

In contrast, four emissions were detected for the irradiated sample (red curve): peak A as a shoulder at 260–270 K and peak B at 300 K and further two well separated peak structures C at 320–340 K and D at 350–380 K which must be related to irradiation-induced traps. TSC activation energies E_{act} were extracted by applying the same heating rate β at each peak temperature T_m using the relation $\ln(T_m{}^4/\beta) = (E_{act}/k) \times 1/T_m$ while assuming temperature-independent capture cross sections for the trap

Table 1. Sulfur-ion irradiation-induced signals in photoluminescence, photo-current and TSC spectroscopy (DD and DA—deep donor and deep acceptor, ET-electron trap, HT-hole trap, the different properties see within the text).

Methode	Energy (eV)	Range (eV)	Interpretation/ References
PL	GL ≈ 2.48	≈2.5	DA: V_{Ga}^{2+} $(V_{Ga}–O_N)^-$ [19]
		2.35–2.54	DA: V_{Ga}^{3-} or N_i^0 or N_{Ga}^- [10, 21]
PC	2.9	2.85–2.93	DA: C_N^- related [23, 24]
		2.9	DA: V_{Ga}–H–O complex [24]
	2.65	2.64	DA: V_{Ga}-related [25]
TSC	C: 0.78–0.82	0.75	HT [27]
		$E_C-(0.8–0.85)$	ET12: DD—Ga_i [28]
	D: 0.91–0.95	$E_C-(0.9–0.95)$	ET13: DA—N_i [28]
		$E_V+0.95$	HT1: DA—$(V_{Ga}–Si)^{2-}$ [28]

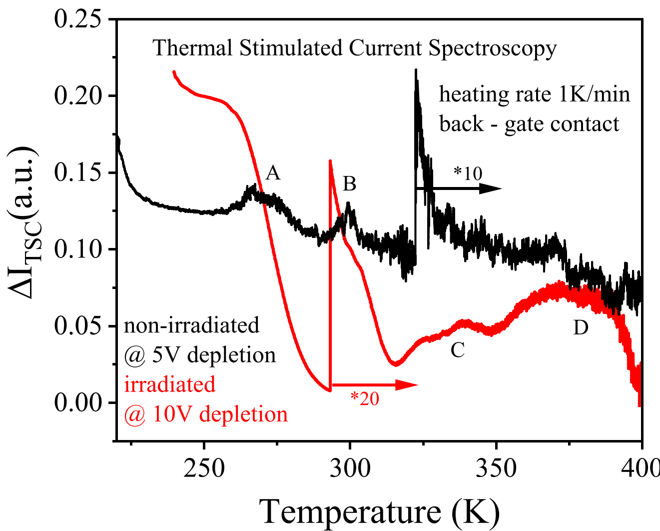

Figure 6. Thermally stimulated current spectra of the non-irradiated and the irradiated sample with the highest dose. Both spectra are magnified vertically by a factor of 20 above 290 K (irradiated HEMT) and a factor of ten above 320 K (non-irradiated), respectively. The TSC peaks A, B, C, and D are described in detail in the text.

states [22]. Accordingly, thermal activation energies of the traps of 0.56 eV (A), 0.65 eV (B), (0.78–0.82) eV (C) and (0.91–0.98) eV (D) were determined. However, it is not possible to distinguish between electron and hole traps (see [22]).

In general, the trap characteristics C and D between 300 K and 400 K were described by many references for samples prepared either by different growth and/or irradiation conditions.

In particular, in non-irradiated AlGaN/GaN HEMTs similar trap emissions between 300 K and 400 K were observed in the TSC spectra [27]. Two defects with activation energies of 0.54 eV and 0.75 eV are assigned to hole traps, while for 0.65 eV an electron trap was concluded from back-gating measurements. These trap energies correlate well with emissions A, C, and B.

According to [28], TSC-emissions C and D in the irradiated sample could also be correlated to ET12 with $E_C-(0.8–0.85)$ eV, ET13 at $E_C-(0.9–0.95)$ eV, HT4 at $E_V+(0.85–0.9)$ eV and HT1 at $E_V+0.95$ eV. For all of these traps, an enhanced peak intensity was found after irradiation with neutrons or ions. Furthermore, Fermi-level pinning between traps ET12 and ET13 takes place at around $E_C-1.0$ eV in heavy neutron-irradiated GaN. In those experiments, ET12 was discussed as a donor-like Ga-interstitial related trap and ET13 as a nitrogen-interstitial related acceptor. Additionally, the hole trap HT1 is described as a dominant trap in MOVPE samples and related to a two-fold negatively charged $(V_{Ga}–Si)^{2-}$complex [28].

Theoretical studies further assign ET12 to a V_{Ga}^{2-} defect and trap emissions at 0.95 eV to an interstitial Ga defect [21].

Table 1 also contains a summary of the trap-related TSC emissions between 300 and 400 K with possible assignments to characteristic defects. All acceptor-like intrinsic defects are described as V_{Ga}-related or other deep acceptor-like intrinsic defects, such as Ga_i, N_i or N_{Ga}.

Please note that the DD and DA states are deduced from experiments conducted at equilibrium conditions, while ET and HT are deduced under non-equilibrium conditions.

4. Conclusion

We have investigated the impact of 75 MeV sulfur ion irradiation on the dual-finger gate and depletion mode HEMTs. The focus of our work was on the impact of the undoped GaN layer and its compensation caused by irradiation. The compensation effect was revealed by a systematic increase in the resistivity both in forward and in reverse directions in the vertical current–voltage characteristics between the gate contact and Si-substrate. Since the non-irradiated undoped GaN buffer layer has *n*-type conductivity, deep acceptors must have been generated to compensate the buffer of the irradiated HEMTs.

The expansion of the lattice in the *c*-direction without broadening of the corresponding ω-FWHM corresponds to only moderate damage to the crystal structure, mainly from the generation of point defects.

As the irradiation induced an additional PL-band within the green spectral region a two-fold charged V_{Ga}-related transition is identified as a possible defect, which is supported by threshold energies of 2.9 eV and 2.65 eV in PC-measurements. These energies have been discussed in the literature as V_{Ga}–O–H complexes acting as acceptors. Such an interpretation for V_{Ga}-related acceptors also holds for the irradiation-induced thermal emission in TSC.

In particular, any allocation of irradiation induced trap emissions and optical transitions to carbon could be omitted.

Other interstitial defects such as Ga_i and N_i or the $N_{Ga}-$ antisite defects are, however, not excluded as they are typical point defects resulting from strong displacement processes as induced by heavy ions. The shallower V_N-defect states and transitions were not detected.

Our results demonstrate the importance of GaN buffer quality for irradiation hardness of the device. The buffer must be optimized for both the HEMT transfer characteristics as well as the avoidance of strong radiation induced changes in the resistivity and number of deep defects. In conclusion, an initial buffer should include as many deep defects as the additional induced defects create minimal changes.

Data availability statement

All data that support the findings of this study are included within the article (and any supplementary files).

Acknowledgments

The authors gratefully acknowledge the funding by the Deutsche Forschungsgemeinschaft (DFG) within projects INST 272/266-1 and INST 272/265-1 and funding of part of this work by the Bundesministerium für Bildung und Forschung (BMBF) under Contract No. 01DN16023.

ORCID iD

H Witte https://orcid.org/0000-0002-2593-0445

References

[1] Neuburger M *et al* 2004 Unstrained InAlN/GaN HEMT structures *Int. J. High Speed Electron. Syst.* **14** 785–90
[2] Dadgar A 2019 GaN-On-Si epitaxy *Encyclopedia of Applied Physics* (New York: Wiley & Son) pp 1–13
[3] Choi F S, Griffiths J T, Ren C, Lee K B, Zaidi Z H, Houston P A, Guiney I, Humphreys C J, Oliver R A and Wallis D J 2018 Vertical leakage mechanism in GaN on Si high electron mobility transistor buffer layers *J. Appl. Phys.* **124** 055702
[4] Lauenstein J-M 2021 Wide bandgap power device radiation reliability *2021 NEPP Electronics Technology Workshop* (*Greenbelt, MD*, 14–17 June)
[5] Granta J, Batesa R, Cunninghama W, Bluea A, Melonea J, McEwana F, Vaitkusb J, Gaubasb E and O'Shea V 2007 GaN as a radiation hard particle detector *Nucl. Instrum. Methods Phys. Res.* A **576** 60–65
[6] Bộas A C V, de Melo M A A, Santos R B B, Giacomini R, Medina N H, Seixas L E, Finco S, Palomo F R, Romero-Maestre A and Guazzelli M A 2021 Ionizing radiation hardness tests of GaN HEMTs for harsh environments *Microelectron. Reliab.* **116** 114000
[7] Pearton S J, Ren F, Patrick E, Law M E and Polyakov A Y 2016 Review—ionizing radiation damage effects in GaN devices *ESC J. Sol. State Sci. Technol.* **5** Q35–Q60
[8] Karlusic M *et al* 2015 Response of GaN to energetic ion irradiation: conditions for ion track formation *J. Phys. D: Appl. Phys.* **48** 325204
[9] Zhang L M, Zhang C H, Zhang L Q, Jia X J, Mac T D, Song Y, Yang Y T, Li B S and Jin Y F 2011 Structural and optical study of irradiation effect in GaN epilayers induced by 308 MeV Xe ions *Nucl. Instrum. Methods Phys. Res.* B **269** 1782
[10] Islam Z, Paoletta A L, Monterosa A M, Schuler J D, Rupert T J, Hattar K, Glavin N and Haque A 2019 Heavy ion irradiation effects on GaN/AlGaN high electron transistor failure at off-state *Microelectron. Reliab.* **102** 113493
[11] Polyakov A Y, Pearton S J, Frenzer P, Ren F, Liu L and Kim J 2013 Radiation effects in GaN materials and devices *J. Mater. Chem.* C **1** 877
[12] Vega N A *et al* 2019 Outstanding reliability of heavy-ion-irradiated AlInN/GaN on silicon HFETs *IEEE Trans. Nucl. Sci.* **66** 2417
[13] Darakchieva V, Monemar B and Usui A 2007 On the lattice parameters of GaN *Appl. Phys. Lett.* **91** 031911
[14] Challa S R, Vega N A, Mueller N A, Kristukat C, Debray M E, Witte H, Dadgar A and Strittmatter A 2021 Understanding high-energy 75-MeV sulfur-ion irradiation-induced degradation in GaN-based heterostructures: the role of the GaN channel layer *IEEE Trans. Electron Devices* **68** 24–28
[15] Ziegler J F, Ziegler M D and Biersack J P 2010 SRIM—The stopping and range of ions in matter *Nucl. Instrum. Methods Phys. Res.* B **268** 11–12
[16] Liu C, Mensching B, Volz K and Rauschenbach B 1997 Lattice expansion of Ca and Ar ion implanted GaN *Appl. Phys. Lett.* **71** 2313
[17] Kucheyeva S O, Williamsa J S and Pearton S J 2001 Ion implantation into GaN *Mater. Sci. Eng.* R **33** 51–107
[18] Boudinov H, Kucheyev S O, Williams J S, Jagadish C and Li G 2001 Electrical isolation of GaN by 1MeV ion irradiation *Appl. Phys. Lett.* **78** 943
[19] Reshchikov M A and Morkoc H 2005 Luminescence properties of defects in GaN *J. Appl. Phys.* **97** 061301
[20] Ito S, Nakagita T, Sawaki N H, Ahn H S, Irie M, Hikosaka T, Honda Y, Yamaguchi M and Amano H 2014 Nature of yellow luminescence band in GaN grown on Si substrate *Jpn. J. Appl. Phys.* **53** 11RC02
[21] Xie Z *et al* 2019 Donor and acceptor characteristics of native point defects in GaN *J. Phys. D: Appl. Phys.* **52** 335104
[22] Orton J W and Blood P 1990 *The Electrical Characterization of Semiconductors: Measurement of Minority Carrier Properties* (New York: Academic)
[23] Klein P B and Binari S C 2003 Topical Review—photoionization spectroscopy of deep defects responsible for current collapse in nitride—based field effect transistors *J. Phys.: Condens. Matter* **15** R1641–67
[24] Wolter M, Javorka P, Fox A, Marso M, Lüth H, Kordos P, Carius R, Alam A and Heuken M 2002 Photo-ionization spectroscopy of traps in AlGaN/GaN high electron mobility transistors *J. Electron. Mater.* **31** 1321
[25] Arehart A R, Corrion A, Poblenz C, Pei Y, Speck J S, Mishra U K and Ringel S A 2008 Deep level optical and thermal spectroscopy in n-GaN grown by ammonia molecular beam epitaxy *Appl. Phys. Lett.* **93** 112101
[26] Jiang W, Nolan M, Ehrentraut D and Dèvelyn M P 2017 Electrical and optical properties of gallium vacancy complexes in ammonothermal GaN *Appl. Phys. Express* **10** 075506
[27] Yang S, Zhou C, Jiang Q, Lu J, Huang B and Chen K J 2014 Investigations of buffer traps in AlGaN/GaN-on-Si devices by thermally stimulated current spectroscopy and back gating measurements *Appl. Phys. Lett.* **104** 013504
[28] Polyakov A Y and Lee I-H 2015 Deep traps in GaN-based structures as affecting the performance of GaN devices *Mater. Sci. Eng.* R **R94** 1–56